Project No. 01-59

# Proposed Enhancements to Pavement ME Design: Improved Consideration of the Influence of Subgrade Soils Susceptible to Frost Heave on Pavement Performance

## APPENDIX 12

INCORPORATION OF DISTRESS CAUSED BY THE FROST HEAVE INTO PAVEMENT DESIGN PROCEDURES

MAY 2023

TABLE OF CONTENTS

## LIST OF FIGURES

## LIST OF TABLES

## 12.1 Introduction

This Appendix discusses the work for incorporating frost heave impact on pavement into the IRI evaluation equation. An updated IRI equation was proposed for the flexible pavement sections with frost actions. The equation is calibrated based on the Monto Carlo analysis results via 1-D model simulations. For the calibration purpose, data collecting and processing, previous IRI model performance evaluation, initial IRI and site factor considerations, and Monto Carlo analysis details were well-reported below. The details of the 1-D model are presented in Appendix 6. Using the collected data in this chapter, a supplement work of IRI empirical equation development was presented in Appendix 13.

## 12.2 Objectives

The study objectives in this chapter are summarized below:

1. Collect and process data needed for the IRI model calibration and 1-D model analysis from LTPP database
2. Evaluate the performance of the MEPDG IRI model for the flexible pavement
3. Discuss the initial IRI, site factor, and age consideration in the IRI model.
4. Calibrate the IRI model using Simplified 1-D model by Monte Carlo analysis

## 12.3 Relative background

The online LTPP database contains climatic data, pavement distress data, pavement parameter data, and measured IRI. These data are not integrated based on a unified time series and can only be downloaded separately. Hence, the team not only collected large amounts of data but also re-organized the data to integrate them with consistent time sequency. The processed data were first used for evaluating current MEPDG IRI model performance, and then were used for the 1-D model Monto Carlo analysis.

## 12.4 Data collection and processing

The data needed for the IRI model calibration (for both the empirical model presented in Appendix 13 and the deterministic model presented in this chapter) were downloaded from LTPP and MERRA initially and then processed by MATALB codes to pick up the data sets suitable for analysis. The information of row data processed by MATLAB was summarized in the Table 12- 1.

**Table 12- 1 The MATALB code processed data information**

| Data type | Data sets | Data source | Data included sections |
|---|---|---|---|
| Site-measured IRI | 19343 | LTPP | 1805 |
| Site-measured rut depth (RD) | 20718 | LTPP | 2572 |
| Site-measured fatigue cracking (FC) and length of transverse cracking (TC) | 12814 | LTPP | 1807 |
| Subgrade Gradation and Atterberg Limit data | 1229 | LTPP | 1229 |
| Annual freezing index | 25625 | MERRA | 2581 |
| Annual total precipitation | 25625 | MERRA | 2581 |
| Section construction and location data | 2581 | LTPP | 2581 |

It was noticed that the dates of site measured IRI records may be different from either the dates of FC, TC, or RD records. Therefore, to take fully advantage of the collected data, it is assumed when the dates of the recorded FC, TC or RD were within ±180 days of the IRI record dates, their dates can be used as same as the IRI recording dates. This assumption is made based on the observation that the distress values such as FC, TC or RD usually do not change appreciably within half a year. Using the site measured IRI dates as the reference, the FC, TC, and RD data with the assumed same dates were sorted via MATLAB code. In addition, the other type of data was also selected by referring to the IRI dates. All sorted and calibration utilized data was summarized in Table 12- 2.

**Table 12- 2 The combined data for IRI equation calibration**

| Data Type | Data Content |
|---|---|
| Site Information | STATE_CODE; STATE_CODE_EXP; SHRP_ID; Date of Construction; Age after Construction; Latitude; Longitude; Construction Number |
| Soil Parameters | NO_4_PASSING; NO_200_PASSING; HYDRO_02; LIQUID_LIMIT; PLASTIC_LIMIT; PLASTICITY_INDEX; wPI; Segregation Potential (SP) of Subgrade |
| Climatic Information | Annual Average Freeze Index; Precipitation |
| Distress Data | International Roughness Index (IRI) Section Average; Initial IRI; HPMS16_CRACKING_PERCENT_AC (%) (AC values); MEPDG_CRACKING_LENGTH_AC (ft/mi) (TC values); Rutting(in) |
| Calculated Result | Age determined SF; IRI increment due to distress; IRI increment due to SF; SF-IRI_0 increment; Model Predicted IRI; IRI Prediction Residual; |

## 12.5 The MEPDG IRI model for flexible pavement

According to MEPDG manual, the equation for new HMA pavements and HMA overlays of Flexible pavements is:

$$IRI = IRI_0 + 0.0150(SF) + 0.400(FC_{Total}) + 0.0080(TC) + 40.0(RD) \quad \textbf{(12- 1)}$$

where $IRI_0$ is the Initial IRI after construction (in/mi), *SF* is the Site factor, $FC_{Total}$ is the Area of fatigue cracking (% of the total lane area). All load related cracks are combined on an area basis. That is, the length of the cracks is multiplied by 1 ft to convert length into an area. *TC* is the Length of transverse cracking (including the reflection of transverse cracks in existing HMA pavements) (ft/mi), and *RD* is the Average rut depth (in). In MEPDG manual, there are three ways (2015, 2018 and 2020) to compute SF:

Method of 2015: $$SF = Age^{1.5}\left[ln\left((Precip+1)(FI+1)p_{02}\right)\right] + ln\left((Precip+1)(PI+1)p_{200}\right) \quad \textbf{(12- 2)}$$

Method of 2018: $$SF = Age^{1.5}\left[ln\left((Precip+1)(FI+1)p_{4}\right) + ln\left((Precip+1)(PI+1)p_{200}\right)\right] \quad \textbf{(12- 3)}$$

Method of 2020: $$SF = Age^{1.5}\left[ln\left((Precip+1)(FI+1)p_{02}\right) + ln\left((Precip+1)(PI+1)p_{200}\right)\right] \quad \textbf{(12- 4)}$$

where, *Age* is the pavement age (yr); *Precip* is the average annual precipitation or rainfall (in); *FI* is the average annual, freezing index ($^{o}$F days); *PI* is the plasticity index of the soil (%);$P_{200}$ is the percent passing the 0.075 mm sieve; $P_4$ is the percent passing the 4.75 mm sieve; $P_{02}$ is the percent of passing 0.02mm. The differences among the above SF equations mainly come from: 1) subgrade soil gradation parameter used for the frost component; 2) the effects of pavement age on the swell behavior of the subgrade. Apparently, such differences can result in different evaluated SF as well as IRI values.

### *12.5.1 The initial IRI*

The initial IRI ($IRI_0$) is an important parameter for the IRI prediction. Theoretically, the initial IRI should be the IRI measured upon the time when road construction is done. However, there typically exist a time gap between the first recorded IRI and construction start dates, which ranges from 1 year up to more than 20 years. Besides, there is no information readily available that can indicate if road maintenance has been performed before the first recorded IRI. Maintenance activities on the surface of pavement usually reduces the site measured IRI values. Hence, the first available site measured IRI value from the LTTP database may not correspond to the true $IRI_0$ as shown in equation (12- 1). Given it is impossible to perform model calibration without true $IRI_0$, the team assumed that the initial IRI is the first available site measured IRI from the database. To avoid the influence of maintenance on the IRI, for road sections where maintenance was conducted, the IRI history is segmented into different time periods where the initial IRI is defined as the first available IRI record right after the maintenance activities of each history segment. This means for a single road section subjected to multiple maintenance activities, the time series data is broken down into pieces with different time sequences. The assumptions about initial IRI are applied for the following IRI calibration.

### *12.5.2 The site factor and age discussion*

In equation (12- 1), the term of 0.015SF represent the IRI increment caused by the site factors including the impact of temperature, precipitation, age, and subgrade soil gradations. Here the site factor determined IRI increment is defined as the $IRI_{sf}$ for the subsequent discussions. Even though it is impossible to directly measure $IRI_{sf}$ on site, according to $IRI_{sf}$ definition, the theoretical filed measured $IRI_{sf}$ can be estimated through subtracting the other measured terms from the measured IRI in equation (12- 1). In the following work, all the site measured $IRI_{sf}$ is evaluated via such back calculation method and hereafter denotes as the back calculated $IRI_{sf}$. The equation of the back calculated $IRI_{sf}$ is expressed by:

$$\text{Back calculated } IRI_{sf} = IRI - [IRI_0 + C_1(FC_{Total}) + C_2(TC) + C_3(RD)] \qquad \textbf{(12- 5)}$$

where $\mathrm{C}_1, \mathrm{C}_2,$ and $\mathrm{C}_3$ are calibration coefficients. For equation (12- 1), $C_1 = 0.4$, $C_2 = 0.008$, $C_3 = 40$.

Age is significant for evaluating the $IRI_{sf}$. According to the MEPDG manual definition, the age should be the time duration starting from the date of road construction. For example, in MEPDG equation (12- 2) to (12- 4), the age is calculated by the date where IRI measurement was conducted minus the construction start date. To evaluate and calibrate the SF in equation (12- 2) to (12- 4), three possible ways were considered to compute age:

1) age is calculated from the pavement construction date
2) age is calculated from the date when pavement was open to traffic
3) age is calculated from the dates of $IRI_0$ is measured

In principle, using pavement age calculated from the date of pavement construction or open to traffic should be more reasonable. It was found if the age starts from the dates of construction or open (the true pavement age), the $IRI_{sf}$ would be significantly larger than the $IRI_{sf}$ using age calculated from the dates of $IRI_0$. Specially, the MEPDG manual method can significant overestimate the IRI after several maintenance due to the existence of the age term in (12- 2) to (12- 4). Therefore, a compromise way, the SF-attenuation method was proposed. This method still uses the age calculated from the pavement construction date, but the age determined SF will not directly used for IRI equation. Instead, the attenuated SF values, the SF of any given age minus the SF on the $IRI_0$ date age, were used. Through this way, the age still follows the MEPDG manual definition, but the SF (also $IRI_{sf}$) value is decreased, which can help to avoid the overestimation of IRI due to maintenance.

Since calibrating SF (or $IRI_{sf}$) is one of the most important targets of the IRI model calibration, it is critical to know how the SF impact the model prediction. Therefore, using 11 different SF calculation methods together with equation (12- 1), the IRI were computed and compared with the site data based on the collected 4877 sets of data. The SF evaluation methods details and the prediction root mean square error

(RMSE) were presented in Table 12- 3. Figure 12- 1 shows the comparison plot of the equation (12- 1) calculated $IRI_{sf}$ via method 9 in Table 12- 3 and the back calculated site $IRI_{sf}$ via equation (12- 1) and (12- 5). Note that the results shown in Table 12- 3 was obtained based on assumption that the $IRI_0$ is the first available IRI recording within any maintenance history duration. According to results in Table 12- 3 and Figure 12- 1, the following findings were obtained:

1) No matter which methods are used to calculate the SF, all the methods tend to overestimate the $IRI_{sf}$ of the AC surface.
2) Using age starting from $IRI_0$ can result in lower average IRI residual, although using age starting from construction is technically more reasonable.
3) Among the SF equations, the 2015 method has the smallest average residual, 2018 method has the largest average residual; 2020 has average residual in the middle.
4) When apply SF-attenuation method to compute SF, the average IRI residual apparently decreased even though the ages were calculated from the starting of construction, not from the dates when $IRI_0$ were measured.
5) The age based on the construction date or date of road open to traffic can cause negligible difference on $IRI_{sf}$, because the time gap between the construction date and the date of road opening to traffic are usually less than 1 year.
6) Overall, results of method 7, 8, and 9 have relatively smaller residuals. Therefore, the SF-attenuation method was recommended to be used to evaluate the SF.

**Table 12- 3 The 9 SF calculation methods and performance comparisons**

| Method # | Age Calculation | SF equation | SF-attenuation method | Prediction error RMSE |
|---|---|---|---|---|
| Method 1 | From the date of $IRI_0$ | 2018 | Not used | 30.77 |
| Method 2 | From construction date | 2018 | Not used | 64.55 |
| Method 3 | From the date of $IRI_0$ | 2015 | Not used | 29.19 |
| Method 4 | From construction date | 2015 | Not used | 45.34 |
| Method 5 | From the date of $IRI_0$ | 2020 | Not used | 30.45 |
| Method 6 | From construction date | 2020 | Not used | 61.79 |
| Method 7 | From construction date | 2018 | used | 34.60 |
| Method 8 | From construction date | 2015 | used | 31.33 |
| Method 9 | From construction date | 2020 | used | 34.09 |
| Method 10 | From date of road opening to traffic | 2018 | used | 34.56 |
| Method 11 | From date of road opening to traffic | 2015 | used | 31.31 |

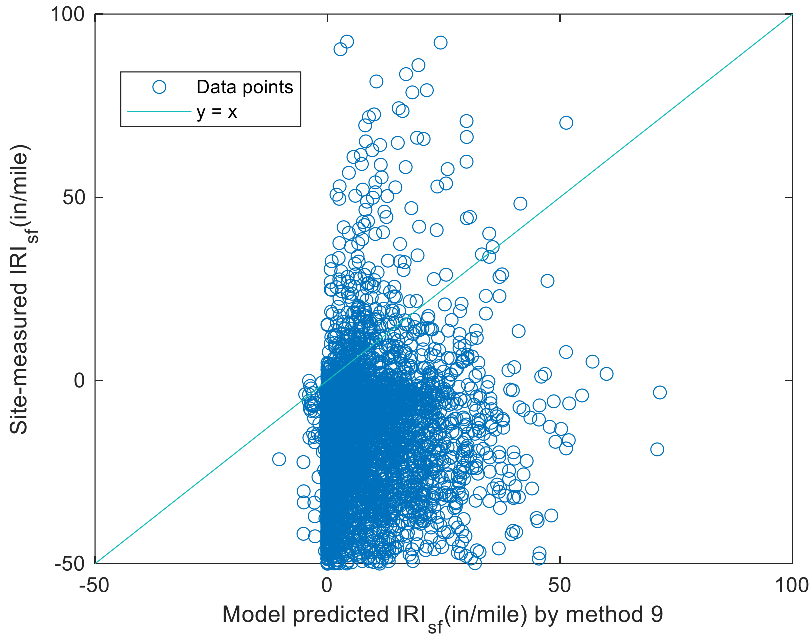


**Figure 12- 1 $IRI_{sf}$ predicted by the current MEPDG method 9 vs. the back calculated site-measured $IRI_{sf}$**

Combining the equations (12- 1) and (12- 5), the back calculated $IRI_{sf}$ histogram chart of more than 9000 sets of data is calculated and shown in Figure 12- 2. According Figure 12- 2, the average back-calculated $IRI_{sf}$ is -16.9 in/mile, which also suggests that current IRI prediction equation (12- 1) overestimates the IRI values for flexible pavements. Note the back-calculated $IRI_{sf}$ can be different after calibrating the coefficients $C_1$ to $C_3$ in equation (12- 5) for the terms corresponding to FC, TC, and RD. This indicates the calibration of coefficients $C_1$ to $C_3$ is one way to improve the underestimated IRI.

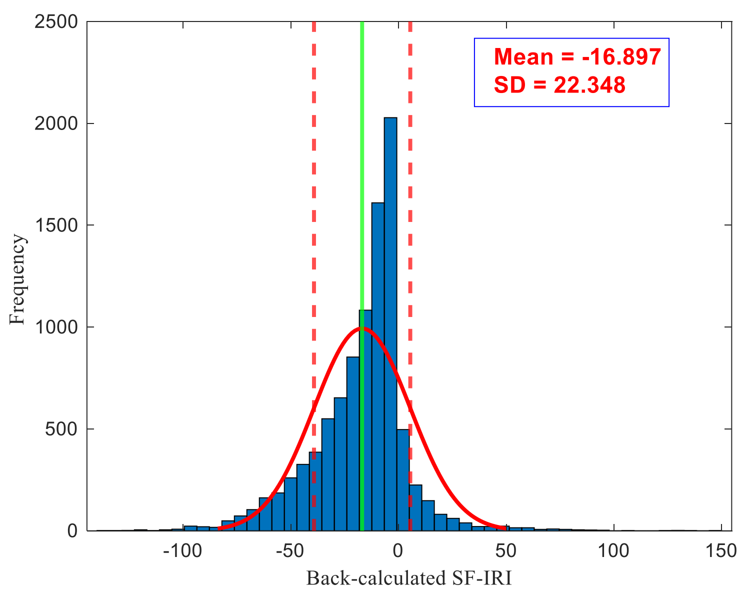


**Figure 12- 2 Back-calculated $IRI_{sf}$ of all 9593 sets of data**

## 12.6 The MEPDG IRI models for frost susceptible flexible pavements

Using equation (12- 1) as well as the SF calculation method 1, 7, 8, 9, 10, and 11 as discussed in Table 12-3, the IRI prediction accuracy (RMSE between site measured IRI and predicted IRI) of these methods was evaluated by considering different segregation potential ($SP_0$) and annual FI conditions, as presented in Table 12- 4. The $SP_0$ and annual FI are the index of the frost susceptibility. Generally, either higher $SP_0$ or annual FI indicates probably severer frost influence. The $SP_0$ is evaluated based on the 1-D model method discussed in Appendix 6 using the subgrade gradation data. The FI data are obtained from LTPP database. Note that IRI were predicted with the following assumptions:

1) The $IRI_0$ used is the first available IRI record within a given maintenance history duration.
2) When the dates of the recorded FC, TC, or RD were within $\pm$180 days of when the IRI. were recorded, their record time were assigned as the same time as the IRI recording time.
3) The IRI increment due to $FC_{Total}$, TC and RD are evaluated based on equation (12- 1)

**Table 12- 4 The performance summary of current IRI model using different SF evaluation methods and frost-susceptibility criteria**

| $SP_0$ (mm^2/C/d) | Annual FI (F-day) | Data set numbers | Method 1 RMSE | Method 7 RMSE | Method 10 RMSE | Method 8 RMSE | Method 11 RMSE | Method 9 RMSE |
|---|---|---|---|---|---|---|---|---|
| >0 | >0 | 4879 | 30.77 | 34.60 | 34.56 | 31.33 | 31.31 | 34.09 |
| >0 | >500 | 1751 | 33.74 | 38.28 | 38.26 | 34.86 | 34.85 | 37.74 |
| >0 | >1000 | 1142 | 35.38 | 39.63 | 39.63 | 36.4 | 36.4 | 39.04 |
| >100 | >1000 | 678 | 33.71 | 37.55 | 37.54 | 34.5 | 34.5 | 36.79 |
| >200 | >1000 | 472 | 34.2 | 37.76 | 37.76 | 34.85 | 34.85 | 36.89 |
| >300 | >1000 | 256 | 38.01 | 41.35 | 41.35 | 38.53 | 38.53 | 40.51 |
| >400 | >1000 | 105 | 44.87 | 48.73 | 48.73 | 44.86 | 44.86 | 47.57 |
| >100 | >1500 | 452 | 33.98 | 37.72 | 37.72 | 34.74 | 34.73 | 36.92 |
| >200 | >1500 | 353 | 34.09 | 37.43 | 37.43 | 34.64 | 34.64 | 36.56 |
| >300 | >1500 | 189 | 38.02 | 40.85 | 40.85 | 38.46 | 38.46 | 40.11 |
| >400 | >1500 | 71 | 45.76 | 48.74 | 48.74 | 45.73 | 45.73 | 47.8 |

According to climatic region classification in LTPP, it is generally believed that the sections located on the east of $96°W$ and north of $36°N$ may suffer more frost influence than the other areas. Hence, the back calculated $IRI_{sf}$ of 3303 sets of data from sections with latitude > 37° and longitude > -96° were collected and analyzed. The back calculated $IRI_{sf}$ results are shown in Figure 12- 3. It seems that the mean and SD difference between Figure 12- 2 and Figure 12- 3 is not apparent. Note that even more than 4000 sets data are from no-frost-susceptible sections in Figure 12- 2, there are 576 sets data have back-calculated $IRI_{sf}$ > 0. The average SP_0, FI, and wPI values among the 576 data set are 557.7 (mm^2/C/d), 137.3(deg F deg days), and 6.54, which imply that the frost susceptibility of soils can affect the $IRI_{sf}$.

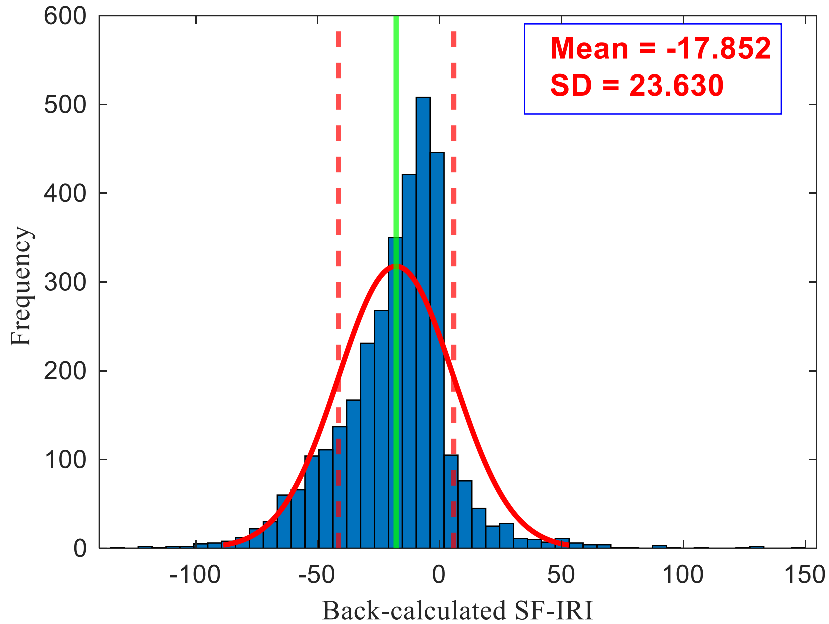


**Figure 12- 3 Back-calculated $IRI_{sf}$ of 3303 sets of data for sections located in latitude > 37° and longitude > -96°**

According to results from the Table 12- 4 Figure 12- 2, and Figure 12- 3, the major findings are:
1) The current MEPDG IRI model generally overpredicts the IRI values for flexible pavement.
2) The higher the frost susceptibility of the road section, the higher the IRI prediction error of RMSE for flexible pavement predicted with the current IRI prediction equation.
3) When the annual FI is larger than a certain value, the higher the segregation potential, the higher the IRI prediction root mean square error (RMSE).
4) When segregation potential is larger than a certain value, the higher the annual FI, the higher the IRI prediction error (by RMSE).
5) Method 7 and 10 (also 8 and 11) showed very close RMSE values, which indicates insignificant difference between using age calculated from construction starting time or the date of opening to traffic. Hence, in the following analyses, only age from construction starting time is used to compute the SF.

In summary, the MEPDG IRI model evaluated $IRI_{sf}$ is not well-estimated. For equation (12- 1), the coefficients $C_1$ to $C_3$, or $IRI_{sf}$ can be calibrated to improve the model performance. For the subsequent work, the Monto Carlo analysis-based method was used to calibrate the model, where a frost heave related term was proposed and used to replace the $IRI_{sf}$ in equations (12- 1). In addition, the coefficients $C_1$ to $C_3$ were also calibrated using the Monto Carlo calculation results.

## 12.7 The IRI model calibration using Simplified 1-D model by Monte Carlo analysis

This part discusses the calibration framework of the method with 1-D model Monte Carlo (MC) analysis. This methodology takes similar measures as the Arizona State University group to calibrate IRI model. This makes the user interface development teamwork compatible and consistent.

### *12.7.1 Methodology of the calibration*

In this study, it is assumed that the difference of temperature and soil property of the pavement at different locations can induce uneven frost heave. The slope of two points along the longitudinal direction of pavement layer is assumed to be caused by such uneven frost heave. If the slope was viewed as a random variable, the statistical dispersion of the slope values is generally assumed to correlated with the pavement distress conditions, where should also be associated with IRI. Such statistical dispersion is assumed to be a function of the standard deviation of frost heave, $\sigma_{FH}$. In addition, the magnitude of the frost heave (or frost depth) should also be associated with the IRI. This conclusion can also easily be drawn from the calibrated empirical model reported in Appendix 13. Therefore, both the mean, standard deviation, and variance of frost heave (or frost depth) of the MC analysis results were studied to find the potential correlations with the IRI.

To be specific, 1000 sets of time series ambient temperature and soil properties were firstly randomly generated as the main inputs of the 1-D model. The randomness of temperature data follows moving weighted average rule. The randomness of soil properties follows beta distributions. The specific beta distributions parameters depend on the soil classification, design level, and the site-measured parameter (such as water content, dry density, and clay percentage). Details about the random parameter generation are presented in Appendix 8. Then, the 1000 sets of the input are assigned to the 1-D model to perform the MC analysis. Each simulated result represents frost heave or depth at one location point. The 1000 sets results indicate 1000 frost have or depth values of different locations. The mean, $\sigma_{FH}$ and $\sigma_{FH}^2$ among the 1000 frost have and depth values were evaluated. The regression was conducted to examine the potential relationship between IRI and mean, $\sigma_{FH}$ or $\sigma_{FH}^2$ of the frost heave or frost depth.

The simplified 1-D model and its MC analysis are integrated by MATLAB code, where the results of model geometry, frost depth vs. date in month, thawing depth vs. date in month, frozen length vs. date in month, frost heave due to water expansion vs. date in month, and frost heave due to segregation potential vs. date in month, can be computed after the level-based inputs are given. The result example of 100 times MC analysis is presented in Figure 12- 4. The time step of the 1-D model is set as one month. Compared with the daily time step, the monthly step calculation has higher computation efficiency and is easier to converge.

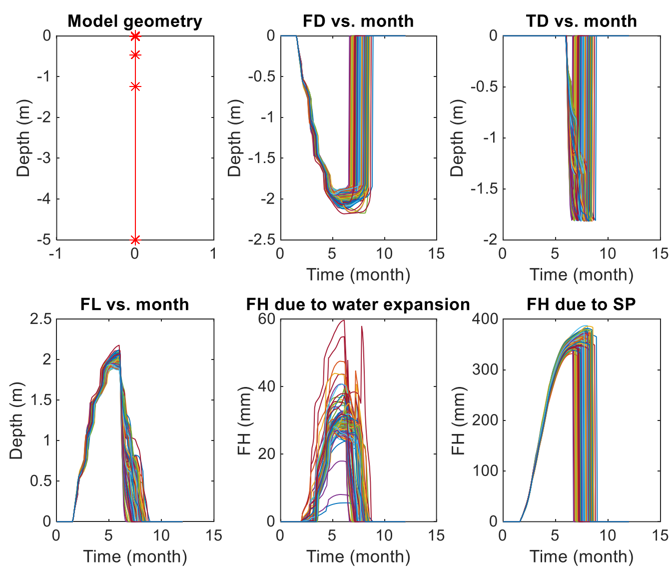


**Figure 12- 4 Simplified 1-D model 100 times MC analysis results example**

### *12.7.2 Temperature prediction model*

For the MC analysis, the randomness of temperature input follows moving weighted average rules. This means the historical temperature will impact the generated random temperature in future. Hence, a temperature prediction model modified based on TMI prediction model of ASU team (see details in Appendix 9) was developed and incorporated in the 1-D model MATLAB code. This temperature model has below characteristics:

1) The model can predict future monthly average temperature based on historical monthly temperature data. At least 20 years of historical temperature data are needed for a design.
2) The model used autoregressive integrated moving average method, which can incorporate the temperature influence of previous months on following months into the prediction.
3) The autoregressive integrated moving average method considers the features of temperature difference between two consecutive month and can generate random temperature increment or decrement within reasonable range and hence can predict the temperature within reasonable range. This means the randomness of temperature can be considered within a reasonable range.
4) To be specific, there are two lag values of the autoregressive integrated moving average method. The lag value of monthly average temperature is set as 2 and lag value of consecutive monthly average temperature difference is also set as 2. The lag values are proposed based on general temperature autocorrelation chart features.

The temperature model needs historical monthly temperature as input. The output of the model is the randomly generated monthly temperature of a given times of MC analysis. The model prediction of 10 times MC analysis example for one section in Colorado is shown in Figure 12- 5. In Figure 12- 5, the monthly temperature from 2001 to 2017 is predicted using historical monthly average temperature from 1972 to 2000. The predicted temperature includes the result of 10 times MC analysis and its average. As shown in Figure 12- 5, the model predicted temperature shows consistent variation trend with historical data and the predicted temperature of all MC analysis are within reasonable ranges.

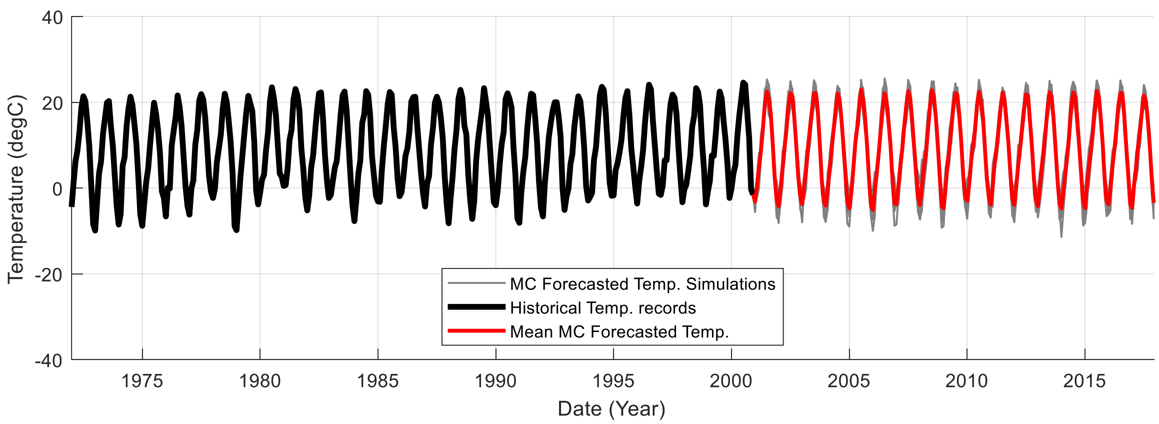


**Figure 12- 5 The model prediction of 10 times MC analysis example section 08-7783 in Colorado**

### *12.7.3 The randomness consideration of the MC analysis*

For the Monto Carlo analysis, the input randomness is contributed to the climatic input uncertainty and subgrade soil property uncertainty. The climatic input randomness only considers temperature stochastic effect. The random temperature values can be predicted by the temperature prediction model as discussed in 12.7.2. The subgrade soil properties uncertainty considers the randomness of dry unit weight ($\gamma_d$), water content (WC), Plasticity Index (PI), percentage passing #200 sieve ($P_{200}$), and percentage of clay ($P_{clay}$). The random soil properties are generated using MALTB code *FH_Beta_Distributions_Fun* and *Random_FH_Soil_Property_Generator* Develoepd by ASU team.

### *12.7.4 Data processing and collection*

Given the limited available data in LTPP, it is found only a Quasi-level 2 Monte Carlo analysis can be performed. Based on the input need and data availability, only 25 sections with AC surface were selected for the MC analysis. The sections are selected following these criteria:

1) At least 5 points of IRI vs. date.
2) All sections must have average maximum FD (evaluated from empirical equation) larger than the pavement thickness.
3) The sections have available distress data including IRI, FC, TC, and RD.
4) The sections have available geometry information, dry density, and water content data of each pavement layer.
5) The sections have available gradation data of subgrade layer.
6) The sections have other available 1-D model needed inputs.
7) For those sections, the missing needed inputs of the 1-D model can be assumed reasonably.
The 25 sections information is summarized in Table 12- 5.

**Table 12- 5 The selected section information of the Quasi-level 2 Monte Carlo analysis**

| STATE_CODE | STATE_CODE_EXP | SHRP_ID | Available data set number |
|---|---|---|---|
| 8 | Colorado | 7783 | 5 |
| 26 | Michigan | 0115 | 5 |
| 26 | Michigan | 0123 | 5 |
| 30 | Montana | 0116 | 5 |
| 30 | Montana | 0119 | 5 |
| 30 | Montana | 0124 | 5 |
| 30 | Montana | 7075 | 6 |
| 30 | Montana | 8129 | 14 |
| 36 | New York | 0801 | 28 |
| 36 | New York | 0802 | 11 |
| 36 | New York | 0859 | 10 |
| 39 | Ohio | 0106 | 7 |
| 39 | Ohio | 0111 | 5 |
| 39 | Ohio | 0160 | 5 |
| 46 | South Dakota | 0803 | 10 |
| 46 | South Dakota | 0804 | 25 |
| 49 | Utah | 1001 | 13 |
| 49 | Utah | 1006 | 5 |
| 53 | Washington | 1007 | 5 |
| 53 | Washington | 1501 | 6 |
| 53 | Washington | 6056 | 6 |
| 56 | Wyoming | 1007 | 12 |
| 83 | Manitoba | 1801 | 17 |
| 87 | Ontario | 1622 | 15 |
| 90 | Saskatchewan | 6405 | 5 |

The pavement geometry and material inputs of the 25 sections are presented in Table 12- 6. The data in Table 12- 6 are collected and compiled from different LTPP data forms. The details are presented below:
1) The pavement geometry information is collected and reorganized based on LTPP data from *TST_L05B*;
2) The dry density data is collected and reorganized mainly based on LTPP form TST_ISD_MOIST. For missing data in TST_ISD_MOIST, the data is supplemented by referring LTPP data form TST_SS08, TST_UG07_SS07_B, TST_UG07_SS07_A. One assumption is made that the base and subbase layers has similarly dry density values. A few sections do not have available base or subbase density data, their values

are estimated using the average density of specific layer type among all the data from the above used LTPP forms.
3) The gravimetric water content data is collected and reorganized mainly based on LTPP form TST_ISD_MOIST. For missing data in TST_ISD_MOIST, the data is supplemented by referring LTPP data form TST_UG10_SS09, TST_SS01_UG01_UG02, TST_UG07_SS07_A. Similar assumption is made as density that the base and subbase layers have close water content values. For sections that do not have available base or subbase water content data, their values are also evaluated using the average water content of specific layer type among all the data from the above used LTPP forms.
4) The gradation data mainly influence the segregation potential calculation. It is assumed the segregation potential of the base or subbase layers is zero. Hence, the analysis only considers the gradation of the subgrade layer. All subgrade gradation data are collected from LTPP data form TST_SS02_UG03 or TST_SS01_UG01_UG02 (The form has data of fine content percentage and latter has gradation data of layers above subgrade). Based on the gradation data, the AASHTO soil classification for the subgrade of the selected sections was determined and used as input to generate the random parameters.
5) The plasticity index data are collected from LTPP data form TST_UG04_SS03

The temperature input is only monthly average temperature before at least 20 years of the simulation start time (usually the date of initial IRI). The used data is VWS of the LTPP database.

**Table 12- 6 The collected pavement geometry and material data of the 25 sections**

| State\|SHRP_ID | STATE_CODE_EXP | LAYER_TYPE_EXP | Average of Thickness (ft) | Dry unit weight (pcf) | WC (%) |
|---|---|---|---|---|---|
| 8\|7783 | Colorado | Asphalt concrete layer | 0.72 | Nan | Nan |
| 8\|7783 | Colorado | Unbound (granular) base | 0.49 | 128.2 | 5.7 |
| 8\|7783 | Colorado | Unbound (granular) subbase | 1.36 | 139.75 | 5.35 |
| 8\|7783 | Colorado | Subgrade (untreated) | 0.00 | 114.84 | 18.33 |
| 26\|0115 | Michigan | Asphalt concrete layer | 0.54 | Nan | Nan |
| 26\|0115 | Michigan | Bound (treated) base | 0.76 | 145 | 4.52 |
| 26\|0115 | Michigan | Subgrade (untreated) | 0.00 | 121.7 | 7.8 |
| 26\|0123 | Michigan | Asphalt concrete layer | 1.43 | Nan | Nan |
| 26\|0123 | Michigan | Subgrade (untreated) | 0.00 | 122 | 6.7 |
| 30\|0116 | Montana | Asphalt concrete layer | 1.45 | Nan | Nan |
| 30\|0116 | Montana | Subgrade (untreated) | 0.00 | 120.9 | 10.25 |
| 30\|0119 | Montana | Asphalt concrete layer | 1.02 | Nan | Nan |
| 30\|0119 | Montana | Unbound (granular) base | 0.36 | 139 | 5.53 |
| 30\|0119 | Montana | Subgrade (untreated) | 0.00 | 122 | 7.5 |
| 30\|0124 | Montana | Asphalt concrete layer | 2.08 | Nan | Nan |
| 30\|0124 | Montana | Subgrade (untreated) | 0.00 | 119.1 | 8.6 |
| 30\|7075 | Montana | Asphalt concrete layer | 0.60 | Nan | Nan |
| 30\|7075 | Montana | Unbound (granular) base | 0.93 | 135.4 | 3.1 |
| 30\|7075 | Montana | Unbound (granular) subbase | 1.73 | 135.1 | 6.2 |

| | | | | | |
|---|---|---|---|---|---|
| 30\|7075 | Montana | Subgrade (untreated) | 0.00 | 122 | 15.57 |
| 30\|8129 | Montana | Asphalt concrete layer | 0.27 | Nan | Nan |
| 30\|8129 | Montana | Unbound (granular) base | 1.90 | 137.9 | 4.48 |
| 30\|8129 | Montana | Subgrade (untreated) | 0.00 | 113.3 | 17.5 |
| 36\|0801 | New York | Asphalt concrete layer | 0.42 | Nan | Nan |
| 36\|0801 | New York | Unbound (granular) base | 0.70 | 136.8 | 2.3 |
| 36\|0801 | New York | Subgrade (untreated) | 0.00 | 131.6 | 5.3 |
| 36\|0802 | New York | Asphalt concrete layer | 0.63 | Nan | Nan |
| 36\|0802 | New York | Unbound (granular) base | 0.83 | 138 | 2.4 |
| 36\|0802 | New York | Subgrade (untreated) | 0.00 | 120 | 8.36 |
| 36\|0859 | New York | Asphalt concrete layer | 0.54 | Nan | Nan |
| 36\|0859 | New York | Unbound (granular) base | 1.04 | 137 | 2.6 |
| 36\|0859 | New York | Subgrade (untreated) | 0.00 | 122.6 | 7.8 |
| 39\|0106 | Ohio | Asphalt concrete layer | 1.22 | Nan | Nan |
| 39\|0106 | Ohio | Unbound (granular) base | 0.32 | 133.8 | 3.8 |
| 39\|0106 | Ohio | Subgrade (untreated) | 0.00 | 124.4 | 9.8 |
| 39\|0111 | Ohio | Asphalt concrete layer | 1.29 | Nan | Nan |
| 39\|0111 | Ohio | Subgrade (untreated) | 0.00 | 122.4 | 9.4 |
| 39\|0160 | Ohio | Asphalt concrete layer | 1.23 | Nan | Nan |
| 39\|0160 | Ohio | Unbound (granular) base | 0.33 | 121.3 | 4.4 |
| 39\|0160 | Ohio | Subgrade (untreated) | 0.00 | 123.4 | 8.4 |
| 46\|0803 | South Dakota | Asphalt concrete layer | 0.38 | Nan | Nan |
| 46\|0803 | South Dakota | Unbound (granular) base | 0.64 | 135.4 | 2 |
| 46\|0803 | South Dakota | Subgrade (untreated) | 0.00 | 110 | 18.6 |
| 46\|0804 | South Dakota | Asphalt concrete layer | 0.59 | Nan | Nan |
| 46\|0804 | South Dakota | Unbound (granular) base | 1.00 | 135.4 | 2.1 |
| 46\|0804 | South Dakota | Subgrade (untreated) | 0.00 | 96 | 15.6 |
| 49\|1001 | Utah | Asphalt concrete layer | 0.49 | Nan | Nan |
| 49\|1001 | Utah | Unbound (granular) base | 0.48 | 130.73 | 2.9 |
| 49\|1001 | Utah | Subgrade (untreated) | 0.00 | 113.1 | 5.73 |
| 49\|1006 | Utah | Asphalt concrete layer | 0.97 | Nan | Nan |
| 49\|1006 | Utah | Unbound (granular) base | 0.66 | 135.4 | 4.9 |
| 49\|1006 | Utah | Subgrade (untreated) | 0.00 | 130.13 | 9.2 |
| 53\|1007 | Washington | Asphalt concrete layer | 0.74 | Nan | Nan |
| 53\|1007 | Washington | Unbound (granular) base | 1.08 | 144.8 | 5.63 |
| 53\|1007 | Washington | Subgrade (untreated) | 0.00 | 119.53 | 13.28 |
| 53\|1501 | Washington | Asphalt concrete layer | 0.36 | Nan | Nan |
| 53\|1501 | Washington | Unbound (granular) base | 0.53 | 140.5 | 5.05 |
| 53\|1501 | Washington | Unbound (granular) subbase | 0.48 | 140.15 | 5.4 |
| 53\|1501 | Washington | Subgrade (untreated) | 0.00 | 104.9 | 21.05 |
| 53\|6056 | Washington | Asphalt concrete layer | 0.73 | Nan | Nan |

| | | | | | |
|---|---|---|---|---|---|
| 53\|6056 | Washington | Unbound (granular) base | 0.94 | 148.1 | 4.05 |
| 53\|6056 | Washington | Subgrade (untreated) | 0.00 | 89.3 | 31.05 |
| 56\|1007 | Wyoming | Asphalt concrete layer | 0.23 | Nan | Nan |
| 56\|1007 | Wyoming | Unbound (granular) base | 0.52 | 127.7 | 5.35 |
| 56\|1007 | Wyoming | Subgrade (untreated) | 0.00 | 119.7 | 12.85 |
| 83\|1801 | Manitoba | Asphalt concrete layer | 0.37 | Nan | Nan |
| 83\|1801 | Manitoba | Unbound (granular) base | 0.47 | 131.7 | 5.4 |
| 83\|1801 | Manitoba | Unbound (granular) subbase | 1.10 | 131.7 | 5.4 |
| 83\|1801 | Manitoba | Subgrade (untreated) | 0.00 | 108.2 | 10.7 |
| 87\|1622 | Ontario | Asphalt concrete layer | 0.48 | Nan | Nan |
| 87\|1622 | Ontario | Unbound (granular) base | 0.56 | 125.3 | 1.7 |
| 87\|1622 | Ontario | Unbound (granular) subbase | 2.19 | 121.8 | 2.5 |
| 87\|1622 | Ontario | Subgrade (untreated) | 0.00 | 112.9 | 10.8 |
| 90\|6405 | Saskatchewan | Asphalt concrete layer | 0.24 | Nan | Nan |
| 90\|6405 | Saskatchewan | Unbound (granular) base | 0.75 | 135.6 | 3.83 |
| 90\|6405 | Saskatchewan | Bound (treated) subbase | 0.21 | 126.8 | 8.25 |
| 90\|6405 | Saskatchewan | Subgrade (untreated) | 0.00 | 127.3 | 3.05 |

### *12.7.5 Assumptions of the analysis*

Since LTPP do not have all needed inputs for any level analysis, the following assumptions are made to take the missing inputs into account:

1) The initial temperature is not available for most sections. The Green-Ampt model is used to estimate the temperature profile at the beginning of the simulation. All simulation starts from January 1$^{st}$ of one year.
2) The initial water content (water content of all layers at the beginning of the simulation) is not available. It is assumed the measured water content in TST_ISD_MOIST (the measurement date is usually different from the simulation start date) is same as the initial water content
3) Not all gradation data for each layer is available. Given the layers above subgrade are usually not frost susceptible, it is assumed that the frost heave mainly occurred in the subgrade soil. Hence, the gradation data of layers above subgrade is not incorporated as inputs in the Monte Carlo analysis.

Therefore, based on the availability of inputs as well as the above assumptions, the Monte Carlo analysis is determined as quasi-level 2 analysis. Such quasi-level 2 analysis is the feasible calculation with the highest accuracy given the limited input conditions.

### *12.7.6 MC analysis discussion*

The MC analysis with 1000 times calculation of each section were conducted for the selected 25 sections with AC surface. The total calculation took 2 and half days. The average time needed for one section of 1000 times calculation is around 1.5 hours. The results include monthly mean and standard deviation values of frost depth (FD), total frost heave (FH), and frozen length (FL). The correlation charts as well as Pearson's coefficients of these results were shown below. It is found that the mean and standard deviation of FD, FH, and FL are generally correlated.

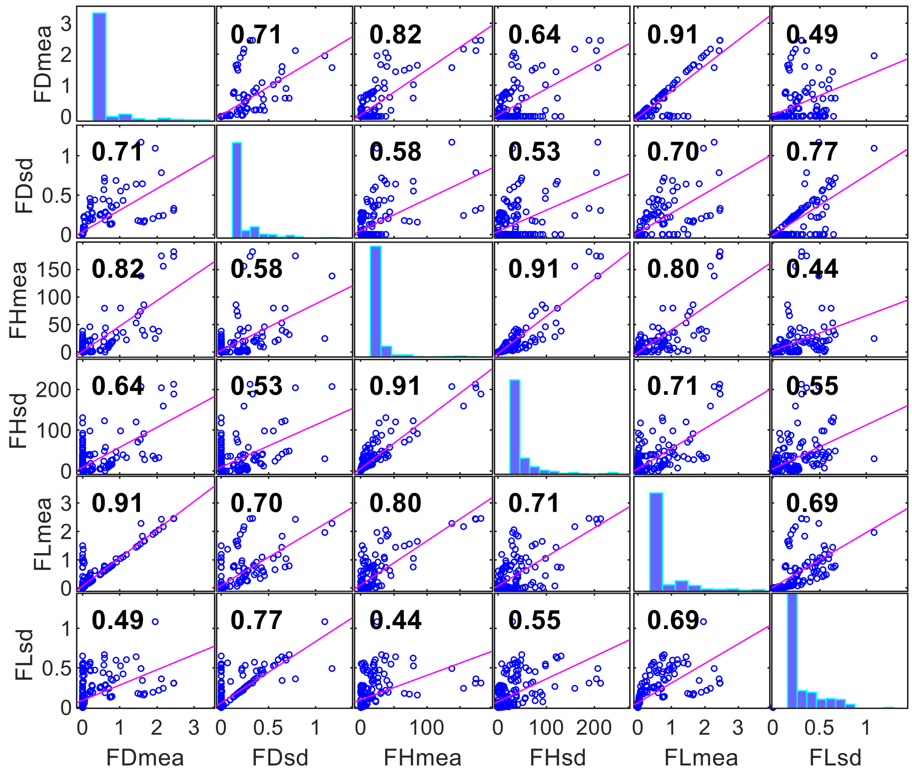


**Figure 12- 6 Monthly mean and standard deviation FD, FH, and FL correlation charts with Pearson's coefficients**

The calibrated IRI model followed previous IRI models of MEPDG, where linear formular were used. Correlation charts with Pearson's coefficients for IRI, initial IRI, FC, TC, rutting, and pavement age are shown below. According to the correlation coefficients, except age, all other parameters were considered in the calibrated model. The parameter age showed very low correlation with IRI. Considering FC and TC is usually correlated with age, hence, the IRI calibration equation did not directly incorporate age in it and is determined by:

$$IRI = IRI_0 + IRI_{FH} + c_2 * FC + c_3 * TC + c_4 * RD \quad \textbf{(12- 6)}$$

$$IRI_{FH} = c_1 * SI_{frost} \quad \textbf{(12- 7)}$$

where $IRI_0$ is initial IRI; $IRI_{FH}$ is frost heave induced IRI increment. $SI_{frost}$ is a term related to statistical index of monthly frost heave (or frost depth) among the Monto Carlo analysis; $c_1$ to $c_4$ are calibration coefficients. The nonlinear least squares solver *lsqcurvefit* in MATLAB was used to regress the coefficients.

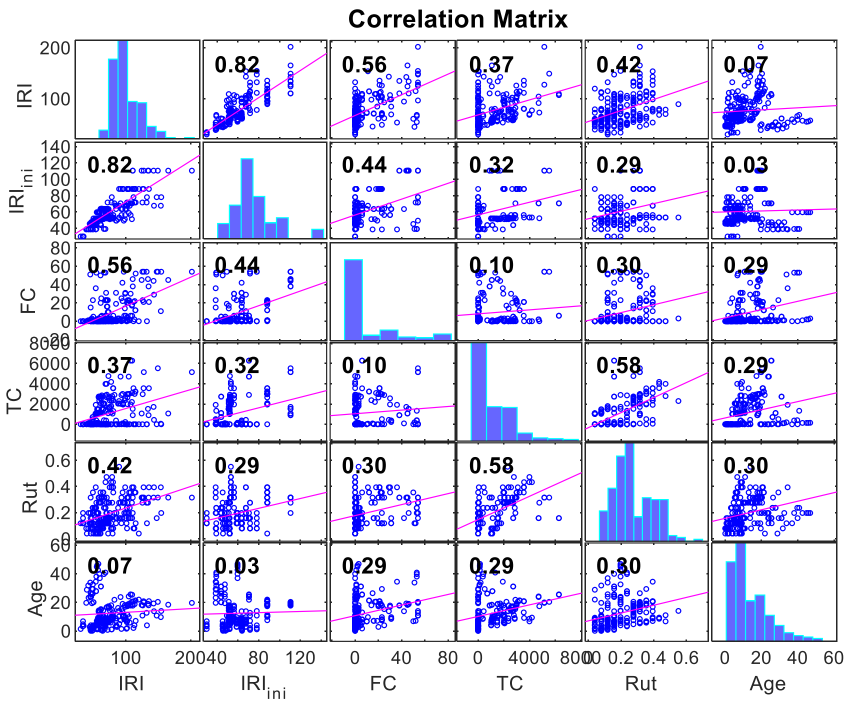


**Figure 12- 7 Correlation charts with Pearson's coefficients for IRI, initial IRI, FC, TC, RD, and age**

The slope difference of pavement surface is believed to be associated with the $SI_{frost}$. The mean, the standard deviation (SD), and the variance ($SD^2$) of the all the MC analysis results of frost depth (FD) and total frost heave (FH) were assigned separately for regression trials to determine the proper $SI_{frost}$. The regression results were summarized in Table 12- 7. According to Table 12- 7, the goodness of fit for the six statistical parameters are very close. In addition, the regressed $c_2$ to $c_4$ values are very close, and the main difference lies in the regressed $c_1$ values. Considering the smallest goodness of fit, the statistical index was then selected as the SD of FH.

**Table 12- 7 The regression results with different statistical parameters**

| $SI_{frost}$ | Goodness of fit: root mean square error | c1 | c2 | c3 | c4 |
|---|---|---|---|---|---|
| Mean of FD (ft) | 14.37 | 0.01 | 0.452 | 0.0014 | 46.70 |
| SD of FD (ft) | 14.30 | 2.15 | 0.455 | 0.0009 | 45.42 |
| Variance of FD (ft) | 14.32 | 0.5 | 0.453 | 0.0011 | 47.04 |
| Mean of FH (in) | 14.26 | 0.01 | 0.443 | 0.0006 | 48.89 |
| SD of FH (in) | 14.23 | 3.12 | 0.455 | 0.0006 | 47.17 |
| Variance of FH (in) | 14.32 | 0.45 | 0.453 | 0.0007 | 48.20 |

Therefore, $IRI_{FH} = 3.12 * \sigma_{FH}$, the calibrated equation is:

$$IRI = IRI_0 + 3.12 * \sigma_{FH} + 0.455 * FC + 0.0006 * TC + 47.17 * RD \quad \textbf{(12- 8)}$$

where $\sigma_{FH}$ is the SD of the simulated frost heave in in.

The 1-1 plot of the calibrated equation is shown below. The 235 data points from the sections as shown in Table 12- 5 were used for the calibration. The $R^2$ of the calibrated equation 12- 9 is 0.75 as displayed in Figure 12-8.

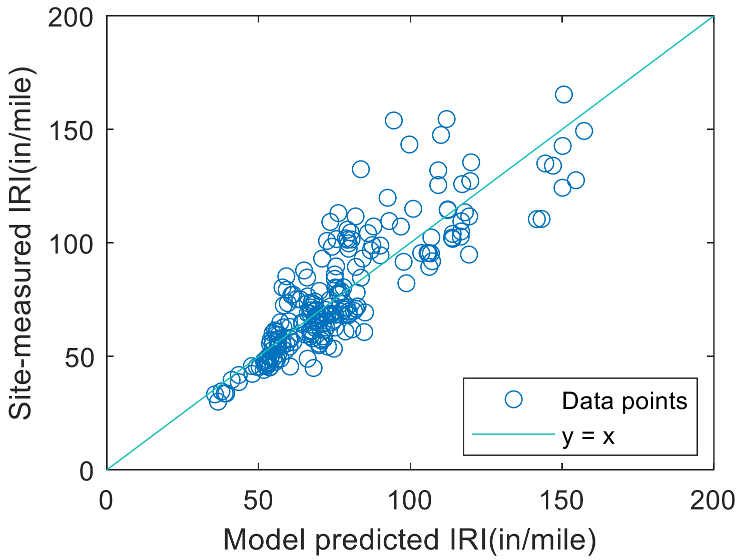


**Figure 12- 8 The 1-1 plot of the calibrated IRI model**